Hole Transport Simulations in p-channel Si MOSFETs

S. Krishnan*, D. Vasileska* and M.V. Fischetti**

* Department of Electrical Engineering,
Arizona State University, Tempe, AZ, 85287-5706, USA
Fax: (480) 965-8058, Phone: (480) 727-7522
skrish2@imap2.asu.edu, vasileska@asu.edu

**Department of Electrical and Computer Engineering
University of Massachusetts, Amherst, Massachusetts 01003-9292
fischetti@ecs.umass.edu

ABSTRACT

Hole transport is investigated in ultrasmall p-channel Si MOSFETs with gate lengths of 25 nm using the Full band Monte Carlo technique. The device simulator couples a 2D Poisson solver with a discretized 6×6 **k.p** Hamiltonian solver that handles the valence band-structure and includes the effect of the confining potential under the gate, thereby providing the subband structure in the channel region. Carriers in the source and drain regions are treated as quasi-3D particles and the band-structure information is included by solving for the eigenenergies of a more compact 6×6 **k.p** Hamiltonian. It is seen that band-structure calculations are needed in order to describe accurately the high field transport in ultrasmall nano-scale MOSFETs.

Keywords: 2D Monte Carlo, Hole transport, six band **k.p**, Valence band-structure

1 INTRODUCTION

Electron transport in Si inversion layers has been the primary subject of research for many years now, but hole transport has been relegated to the background mainly due to the complex valence band-structure in Si. Hole transport is affected by the warping and anisotropy of the valence bands and the band-structure cannot be approximated with an effective mass picture or with an analytical band model. The advent of alternate device structures [2-4] aimed at boosting the speed and density of VLSI circuits however, seems to have revived interest particularly so because the performance mismatch between *n* and *p* channel devices may vanish as one enters the quasi-ballistic regime. As the gate length of the MOSFET is scaled down into the deca-nano regime for improved performance and density, the requirements for body-doping concentration, gate oxide thickness, and source/drain (S/D) doping profiles to control short-channel effects become increasingly difficult to meet when conventional device structures based on bulk silicon (Si) substrates are employed. The heavy channel doping required to provide adequate suppression of short-channel effects results in degraded mobility and enhanced junction leakage. The aggressive reduction of the SiO_2 gate dielectric thickness for reduced short-channel effects and improved drive current leads to increased direct tunneling gate leakage current and standby power consumption, and also raises concerns regarding the gate oxide reliability. To address these issues, important alternate device technologies proposed are buried channel strained SiGe p-channel MOSFETs [3] and surface channel strained Si [4]. There is considerable merit in pursuing strained SiGe on SOI technology as not only subsurface leakage currents are eliminated, but more importantly, there are strong indications that compressively strained SiGe not only increases the hole mobility, but also enhances the hole velocity overshoot and improves the effective saturation velocity.

Even as we mention these device technologies which need to be properly investigated, the fact remains that there is to the best of our knowledge, no simulator which can properly model hole transport in conventional *p*-channel Si MOSFETs because of the complicated nature of the valence bands. To address this issue, we present a new way of incorporating band-structure and quantum effects on hole transport in conventional Si p-channel MOSFETs. This is achieved by coupling a 2D Poisson–1D discretized 6×6 **k.p** Hamiltonian solver self-consistently to the Monte Carlo transport kernel. The scattering rates in our calculation evolve as a function of simulation time because the confining potential changes and therefore the subband structure changes. This in turn affects the scattering rates which have to be updated frequently in our calculation. The results presented in this paper include only phonon scattering in the full band model. Effects of surface roughness and Coulomb scattering mechanisms will be presented at the conference. It is important to note that our approach is generic and can easily be extended to model strained layer MOSFETs mentioned above by incorporating an additional strain Hamiltonian into the band-structure kernel.

2 VALENCE BAND-STRUCTURE

2.1 E-K Dispersion

The hole band-structure is calculated using the **k.p** method Hamiltonian which is given by

$$\mathbf{H}=\begin{bmatrix}\mathbf{H}_{\mathbf{k.p}} & 0\\ 0 & \mathbf{H}_{\mathbf{k.p}}\end{bmatrix}+\mathbf{H}_{\mathbf{so}}+\mathbf{I}V(z), \qquad (1)$$

where $\mathbf{H_{k.p}}$ and $\mathbf{H_{so}}$ are the 6×6 **k.p** and spin-orbit Hamiltonians respectively, **I** is a 6×6 identity matrix, V(z) is the confining potential along the device depth [5]. Replacing the vector k_z with its operator notation as k_z=-i∂/∂z, and using a finite difference discretization [5], equation (1) can be recast into an eigenvalue equation for the eigenenergies in the x-y plane, for different values of the in-plane **K**-vector, $\mathbf{K}_{\|}$(kx,ky).The solution of the eigenvalue problem involves the diagonalization of a tridiagonal block matrix whose rank is given by $6\times N_Z$, where N_Z is the number of mesh points along the depth direction. For the 3D (bulk) carriers in the source and drain, we only have the first two terms of equation (2). This 6×6 Hamiltonian can easily be diagonalized to give the eigenvalues of 3D carriers at (kx, ky, kz).

2.2 Density of states

To include carrier scattering within the transport kernel, the density of states of the system (2D and 3D) are required. For the 2D case, we tabulate the in-plane **K**-vector, $\mathbf{K}_{\|}$, as a function of carrier energy (ε_{2d}), band (ν) and subband (n) indices, and the in-plane azimuth angle(ϕ). For the 3D case, the K-vector, $\mathbf{K}_{3D}$ is tabulated as a function of carrier energy (ε_{3d}), band index (ν), and the azimuth (ϕ) and elevation (θ) angles. In order to set up the inverse problem, the discretized eigenvalue equation (1) for the 2D system can be recast into a eigenvalue equation for $|\mathbf{K}_{\|}|$ [5] as shown by the following equation, where $\mathbf{D_n}$ operates on $|\mathbf{K}_{\|}|^{\mathbf{n}}$.

$$\begin{bmatrix}\mathbf{0} & \mathbf{I}\\ -\mathbf{D}_2^{-1}.[\mathbf{D}_0-\mathbf{I}E] & -\mathbf{D}_2^{-1}.\mathbf{D}_1\end{bmatrix}\begin{bmatrix}\psi_K\\ \psi_K^{(1)}\end{bmatrix}=K\begin{bmatrix}\psi_K\\ \psi_K^{(1)}\end{bmatrix} \qquad (2)$$

Since ε_ν^n(kx,ky) is quadratic in $|\mathbf{K}_{\|}|$, the problem involves diagonalizing a matrix whose rank is twice as large as that of the discretized **k.p** Hamiltonian, i.e. $12\times N_Z$. In the 3D case, using a similar technique, one can show that the problem involves diagonalizing a matrix whose rank is twice that of the **k.p** Hamiltonian, i.e. 12. Thus, for the 3D case, one can tabulate the values initially and these can be used throughout the simulation. The computational complexity for the 2D case led us to make the following simplifying assumptions.

Using a sufficiently high vertical electric field ~5MV/cm, a triangular test-potential was generated and used to tabulate the dispersions and density of states (DOS) of the ground state subbands in each band (heavy-hole HH, light-hole LH and split off- SO). It was then assumed (eq. (3)) that for the case of a real confining potential in the device, the dispersions in each subband for a particular band would be given by the tabulated (triangular-well) dispersion of the ground state subband of the corresponding band, thus allowing us to capture the basic features of subband anisotropy, warping and nonparabolicity. The only effect of the 'real' confining potential in the device would be the translations of the dispersions on the energy axis by the subband energies at the X point.

$$\varepsilon_\nu^n(k_x,k_y)\approx[\varepsilon_\nu^0(k_x,k_y)-\varepsilon_\nu^0(0,0)]+\varepsilon_\nu^n(0,0) \qquad (3)$$

For the inverse problem, a similar approach is used. The triangular test potential is used in the inverse solver, equation (5), in order to tabulate the in-plane **K**-vectors $\mathbf{K}_{\|}^{n,\nu}(\varepsilon_{2d},\phi)$ for a set of chosen (ε_{2D},ϕ). Having so tabulated in-plane **K**-vectors for the lowest subband in each band, we assume that the same dispersion holds also when employing the actual device potential for all the subbands of the given band.

$$K_{\|}^{n,\nu}(\varepsilon_{2D},\phi)\approx K_{\|}^{0,\nu}(\varepsilon_{2D},\phi) \qquad (4)$$

3 BAND-STRUCTURE CALCULATION

The Monte Carlo particle based simulator handles the transport of holes through the device. Having calculated the hole band-structure in the contacts and the active device region *i.e.* under the gate, the quantum mechanical hole density in the channel, is calculated self consistently with the Poisson equation and the 2D band-structure code. Holes are then initialized in real space based on the local carrier density and their energy is initialized by assuming a thermal distribution. The present version of our simulator accounts only for phonon scattering within the isotropic approximation [5], but uses overlap factors calculated from the actual eigenfunctions in each subband. As the carriers drift under the influence of the electric field due to the applied bias, the confining potential changes and this in turn changes the eigenenergies and the eigenfunctions. As a result, the scattering rates must be updated frequently during the simulation. Within the scope of the current model we have assumed the holes to be quasi 3D particles in the source and drain regions and have used appropriate models to treat these boundary conditions effectively**.** When converting a bulk (3D) Monte Carlo particle into a low-dimensionality (2D) particle occupying a subband in the inversion layer, the difference between the carrier energy ε_{3D} and the in-plane kinetic energy ε_{2D} gives the subband energy ε_ν^n. The carrier subband is then determined by choosing a subband with the minimum error in subband energy and ε_ν^n, the calculated energy. In the opposite case of converting a 2D-particle into a bulk carrier, the 3D carrier energy is given by $\varepsilon_{3D}=\varepsilon_{2D}+\varepsilon_\nu^n$. By scanning the

elevation angle θ from the tabulated values of the 3D **K**-vector and preserving the in plane azimuth ϕ, the $\mathbf{K_{3D}}$ vector which minimizes the error in the magnitude of the in-plane $\mathbf{K_{2D}}$ vector is chosen as the 3D carrier momentum of the bulk particle.

3 RESULTS

The isosurfaces of the lowest Heavy, Light and Split off subbands, for the case of the triangular test potential are shown in Figure 1. Note the strong warping of the heavy hole band when compared with the fairly regular shapes for the light hole and the split off bands which makes it extremely difficult for analytical band models to describe the valence band-structure accurately. The hole-density of states is determined by performing a surface integral over these isosurfaces and these are then used to determine the carrier scattering rates in the channel. Similar surfaces in 3D for the HH, LH and SO bands are shown in figure 2. It can be seen that the HH band is very warped and the LH is lightly warped while the SO band has a much more regular shape.

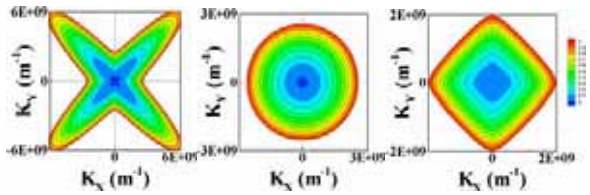

Figure1. Isosurfaces of the lowest lying HH, LH and SO subbands on a (001) oriented substrate.

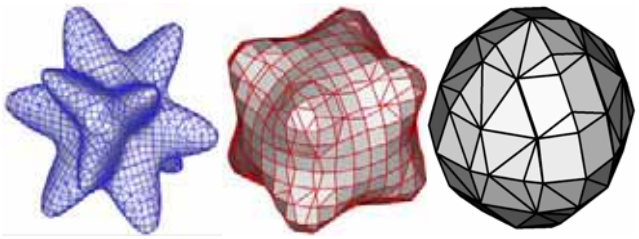

Figure2. Equienergy surfaces for HH, LH and SO bands. The energy is 50 meV below the Γ point.

The density of states for the confined carriers is shown in figure 3. The deviation of the density of states obtained by a full band calculation from a regular step- like profile expected out of an effective-mass type approximation is clearly seen in the case of the light hole and split off bands, whereas the heavy hole density of states looks more like a step function.

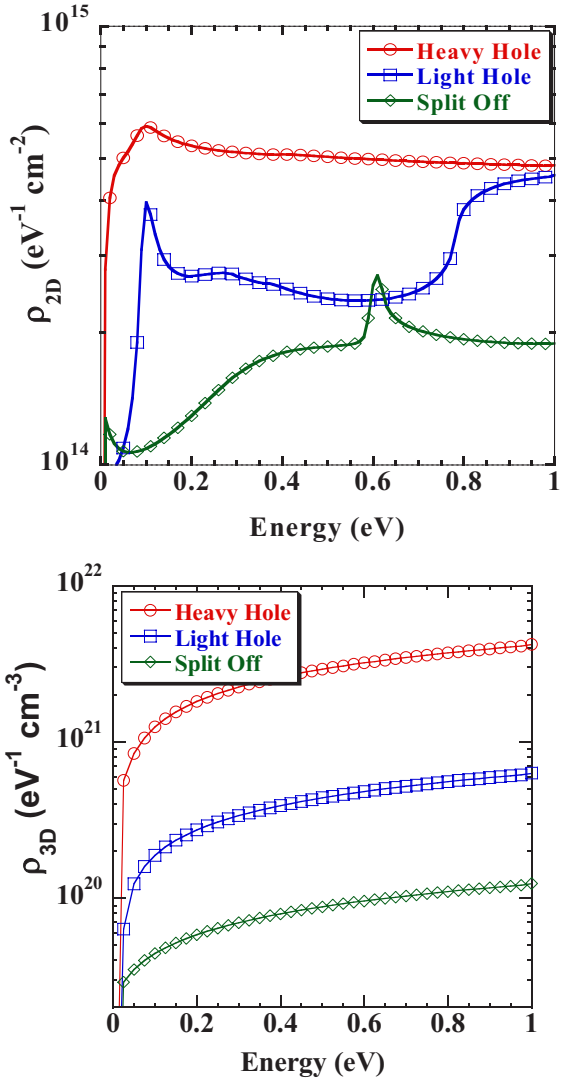

Figure3. Density of States for (top panel) channel (prototypical triangular test potential) and bulk (3D) carriers (bottom panel) respectively using six band **k.p** calculations.

The output characteristics of a 25 nm p-channel conventional Si MOSFET are shown in Figure 4. Significant DIBL is seen in the output characteristics in this case. Only phonon scattering (acoustic and optical phonons) are included in this calculation. An equivalent effective mass two band (Heavy and Light Hole bands) model with similar scattering mechanisms included, underestimates the current by about 14%. Thus it is clear that effective mass approximations are not reliable and therefore band-structure calculations are required to accurately predict the output current under high field transport conditions in nano-scale MOSFETs.

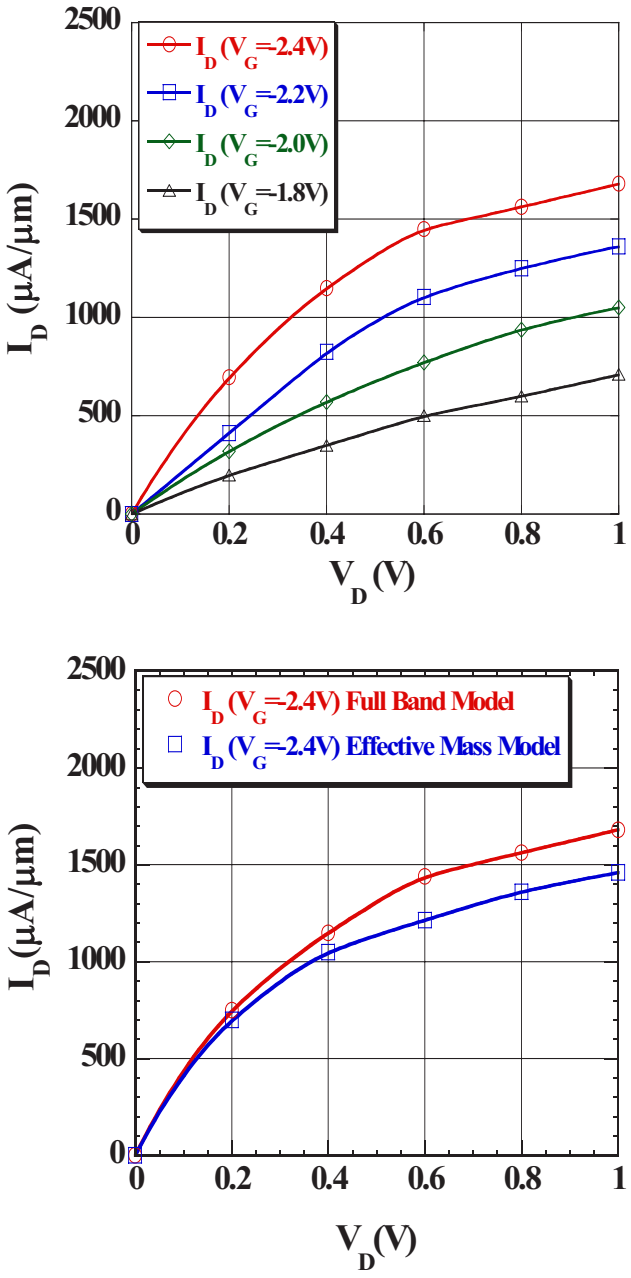

Figure4. Output characteristics of a 25 nm p-channel Si MOSFET calculated using the full band (top panel) and the effective mass (bottom panel) model.

REFERENCES

[1] S. Takagi A. Toriumi, M. Iwase and H. Tango, "On the universality of inversion layer mobility in Si MOSFET's: Part I - Effects of substrate impurity concentration", *IEEE Trans. Electron Devices* **41**(12), 2357 (1994).

[2] P. M. Garone V. Venkataraman, and J. C. Sturm, "Hole mobility enhancement in MOS-gated Ge_xSi_{1-x}/Si heterostructure inversion layers", *IEEE Electron Device Lett.* **13**(1)**,** 56 (1992).

[3] N. Collaert, P. Verheyen, K. De Meyer, R. Loo, M. Caymax, "50 nm high performance strained Si/SiGe pMOS devices with multiple quantum wells", *IEEE Trans. Nanotechnology* **1,** 190 (2002).

[4] R. Oberhuber, G. Zandler, and P. Vogl, "Subband structure and mobility of two-dimensional holes in strained Si/SiGe MOSFETs", *Phys. Rev. B* **58,** (15), 9941 (1998).

[5] M.V. Fischetti, Z. Ren, P. M. Solomon, M. Yang, and K. Rim, "Six-band k·p calculation of the hole mobility in silicon inversion layers: Dependence on surface orientation, strain, and silicon thickness", *Journal of Applied Physics* **94**(2), 1079 (2003).